Aerodynamic shape optimization of a short medium range blended wing body aircraft

Quentin Bennehard

56th 3AF International Conference on Applied Aerodynamics
28 – 30 March 2022, Toulouse - France

FP26-AERO2022-bennehard

AERODYNAMIC SHAPE OPTIMIZATION OF A SHORT MEDIUM RANGE BLENDED WING BODY AIRCRAFT

Quentin Bennehard [(1)]
[(1)] *ONERA, Université Paris-Saclay, 8 Rue des Vertugadins 92190 Meudon (France),*
Email: quentin.bennehard@onera.fr

ABSTRACT

This work presents the aerodynamic shape design and optimization of a short medium range blended wing body configuration. It relies on previous activities performed at ONERA that led to a fuel efficient planform obtained from a dedicated Overall Aircraft Design process. Starting from this planform, the airfoil shape and the twist law of the glider configuration are optimized. A new optimization chain allows automatizing unstructured mesh generation on a parametric geometry. Using this new chain based on a parametric geometry and unstructured Euler simulations, gradient-based optimizations are done using a finite difference approach. RANS evaluations are then conducted on the optimized configuration to assess the aerodynamic performance benefits in terms of lift over drag ratio (one count improvement, while satisfying the trim condition). Finally, the first design iterations to integrate modern turbo-fan engines using boundary layer ingestion are presented.

1. INTRODUCTION

1.1. Context

While air traffic is expected to continue increasing after the end of the Covid crisis, massive gains are necessary for the aeronautics industry to meet the targets set to limit climate change. In this light, optimizing existing aircraft configurations could not be sufficient anymore, and exploring new configurations along with new propulsion technologies are now a necessity. The Blended Wing Body (BWB) concept is the focus of the current paper. This aircraft layout has already been widely studied because it offers great aerodynamic benefits compared to the traditional tube and wing configuration. While new engine technologies are explored (hydrogen or hybrid electric propulsion), the greater interior volume offered by the BWB geometry is also a key advantage. The present work focuses on the conception and optimization of a BWB aircraft suitable for short medium range mission, segment serviced today mainly by the A320 and the B737.

The literature is extensive on the BWB geometry for long-range mission, as it is on this type of mission that the better aerodynamic performance during cruise translates in a greater fuel economy. Liebeck [1] conducted a comprehensive design review of a 450 pax BWB. He demonstrates that the aerodynamic gain mainly comes from a 33% reduction of the wetted surface compared to the traditional tube and wing configuration. His work also deducts a fuel burn per seat reduction of 32%, coming from the great synergy offered by the BWB configuration. Indeed, one wing body ensures payload housing, control, structural and aerodynamic functions. Liebeck also highlights that the main aerodynamic challenge of this configuration lies in the central body. In this part, the geometry is supposed to generate lift at a moderate angle of attack to keep the passengers deck levelled. These requirements, suggest using airfoils having a positive aft camber. However, a positive aft camber airfoil generates a pitch down moment. Without a tail stabilizer and trailing edge surface deflections, it is then challenging to trim the configuration during cruise. Therefore, considering these constraints and the great number of potential geometric variables, the conception of a BWB shape is a good candidate to apply aerodynamic shape optimization. Great progresses in this field have been made in the last decades. Lyu and Martins tackle such a problem in [2], on a large BWB. They use adjoint RANS based optimization and they achieve to obtain a configuration with a lift over drag ratio (L/D) of 21.9. Meheut and al. [3] used the same kind of setups to optimize a BWB subjects to low speed rotational take off constraint.

In his work, Liebeck also suggests that the BWB configurations could be scaled laterally to derive smaller configuration from a large one. Short-medium range trip represents the majority of the air traffic, and are responsible for 40% of its CO2 emissions [4], which

points out the need for a technological shift on this segment as well. On this type of aircraft, considering a shorter chord length and the fact that the mean human being height is constant, the relative thickness of the central airfoils needs to be increased. In theory, this deteriorates the aerodynamic performance of the aircraft. It is then difficult for a thick airfoil to achieve a significant lift at low drag while keeping a low angle of attack. This fact has been highlighted in the work of Kanazaki et al [5].

1.2. Previous work at ONERA

The current work is based on a multi-disciplinary optimization (MDO) of a short-medium range BWB carried out at ONERA in the frame of the European project NACOR. This MDO uses an Overall Aircraft Design (OAD) process developed since 2015 at ONERA [6]. It is constituted by six disciplinary modules: Aircraft Geometry, Propulsion, Aerodynamics, Structure & Weight, Mission & Performance and Handling Qualities. A description of the low level Aerodynamics Module is given in [7].

The top-level aircraft requirements (TLAR) considered for this MDO are the following:

- Payload of 150 pax with 90 kg per pax
- Range of 5100 km
- Mach 0.78

The process allows exploring a great variety of BWB planforms. A MDO problem is defined with objective to minimize the mission fuel weight, the main constraints being the take-off distance, the climb duration and the handling qualities. The results of the MDO can be seen Figure 1 and Table 1. The resulting configuration has been named SMILE (Small – Medium range Integrated Light and Efficient aircraft). Its planform constitutes the starting point of the work presented here after. The OAD process also gives the size and arrangement of the pressurized zone, as seen Figure 2.

Table 1. SMILE configuration mass breakdown

Item		Weight (kg)	% MTOW
OEW		36042	58.8 %
PW		13500	22.0 %
FW	SMR Mission	9091	14.8 %
	Reserve	2669	4.4 %
MTOW		61303	100 %

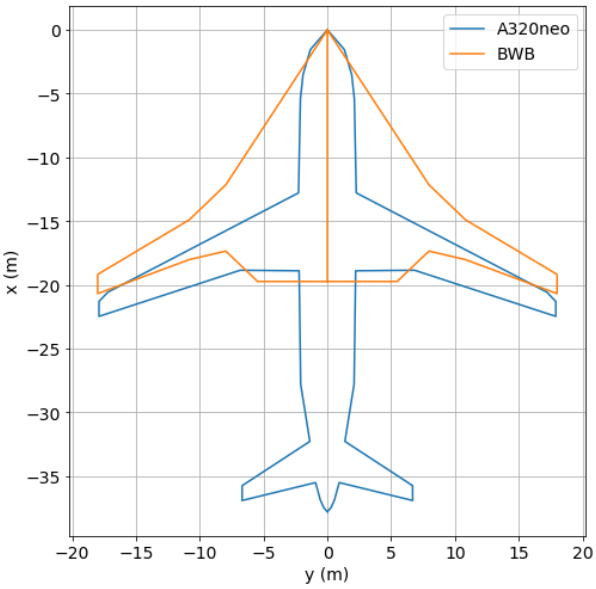

Figure 1. Planform of the BWB obtained by MDO, compared to the planform of the Airbus A320 neo

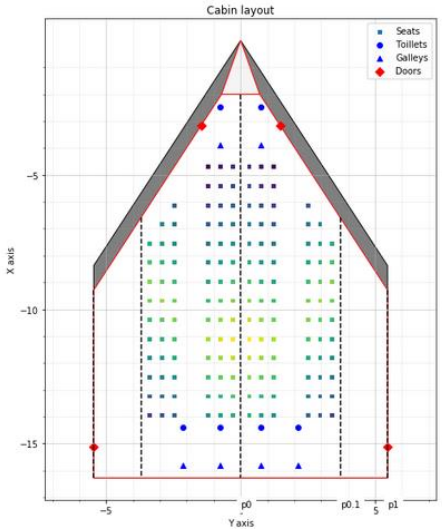

Figure 2. Cabin layout of the BWB configuration. Cargo holds are situated on both sides of the passenger cabin.

The objective of this work is hence to obtain an efficient 3D aerodynamic shape, starting from the planform obtained by the MDO. Engine integration is first not taken into account, as the objective is first to get an efficient glider shape.

This article is organized as follows. First the optimization chain and the baseline geometry are presented. In section 3, the different optimization problems treated are presented. Section 4 discusses the optimization results. Section 5 briefly tackles the challenges observed in engine integration with boundary layer ingestion, followed by the conclusions.

2. DESIGN METHODOLOGY

2.1. Optimization chain

The optimization chain used in this work is an adaptation of the Computational Aircraft Prototype Syntheses (CAPS) chain developed by the MIT [8]. Its components are described Figure 3. Usage of this chain is new at ONERA, especially in an optimization context.

First, the chain includes a fully parametric Computer Aided Design (CAD) module: Engineering Sketch Pad (ESP) [9]. In this work, ESP was retained because it creates a completely parametric geometry. The parameters used to define the shape can then be directly used as design variables of an optimization problem. Furthermore, as it possesses a CAD engine based on Open Cascade, ESP can easily compute the volumes and intersections of complex forms, allowing to easily handle the internal volume constraint of the BWB.

Second, an inviscid or viscous unstructured mesh can be generated automatically on the geometry, leveraging Pointwise scripts [10]. Viscous layers are generated using the T-Rex capability of Pointwise.

On the obtained mesh, the open source flow solver SU2 [11] is then used to solve the aerodynamic field around the shape. SU2 can solve the Euler or RANS equations. For the last ones, the Spalart-Allmaras turbulence model is used. The chain has also be made compatible with the elsA code (ONERA-Airbus-Safran property) [12], using its unstructured capabilities.

Lastly, the in-house ONERA post process tool Far Field Drag (FFD) [13] is employed to extract and decompose the aerodynamic coefficients of the shape. These four steps are run automatically thanks to Python scripts, adapted from the CAPS chain.

An optimizer is coupled to this automatic process, in order to be able to solve the optimization problem. The choice was to use the Dakota Toolbox and the gradient based optimizer DOT MMFD (Modified Method of Feasible Directions) [14]. A gradient-free optimizer is more capable of finding the best minimum in a case of a problem with multiple local minima. However, the high number of functions calls made the use of this type of optimizer infeasible in this case where expensive CFD codes and large number of design variables are used. Rapid convergence of gradient based methods are the main motivation behind their usage, especially when they are combined with heavy CFD codes.

Even if SU2 and elsA have an ajdoint capability, the adjoint information is not fully propagated yet through the mesh and CAD processes. In this case, gradient values were then obtained via finite difference computations. The optimization chain can either be used by solving the Euler flow equations or the RANS ones, at the only cost of computer loads increase.

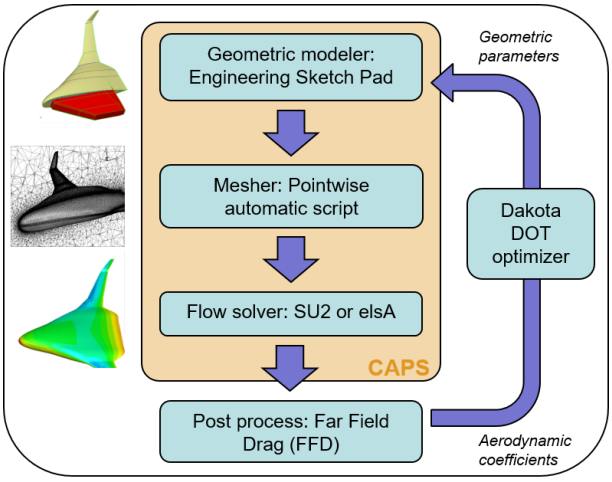

Figure 3. Overview of the optimization chain

2.2. Baseline geometry

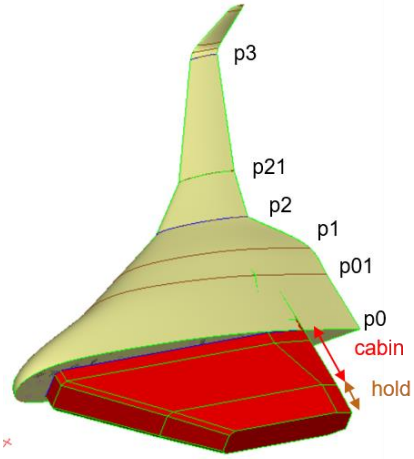

Figure 4. BWB half geometry (in beige) and half geometry of the pressurized volume (in red)

From the given planform presented in Figure 1, a tri-dimensional model was created. The geometry is defined by six sections, named p0, p01, p1, p2, p21 and p3, as seen on Figure 4. On the three central sections, modified four digit NACA airfoils were used. These airfoils were modified “by-hand”, to accommodate the internal pressurized volume. On the outer wing, supercritical airfoils were used, re-using airfoils designed for the ONERA NOVA concept [15]. The central part of the wing is then defined by a cubic interpolation between the sections p0 to p2, preserving a C2 continuity at the intermediate sections. The rounded nose was obtained by imposing a normal tangent at the symmetry plane. The

outer wing is defined by a linear interpolation between the last three sections p2 to p3. A two degrees dihedral angle is added on the outer wing to improve dynamic stability. In addition, winglets are added at the wing tip. They are quite large with a height of 2.5 m, as they contain rudders (not modelled in the CFD simulations) helping the lateral control of the aircraft.

The main geometric parameters are given in Table 2. Since no planform modification will be done, they remain constant for the optimized designs. The centre of gravity is referenced by its position along the longitudinal axis, the origin being at the aircraft nose.

Table 2. Main geometrical characteristics of the BWB SMILE

Mean Aerodynamic chord	12.109 m
Reference surface	268.602 m²
Span	37.73 m
Centre of gravity	12.29 m

The twist law of the baseline was determined iteratively to obtain a configuration achieving the lift needed without a high wave drag penalty. However, in this first manual design loop, it was not possible to find a configuration that achieves the trim condition at the cruise point. The optimization problem considered here after will mainly have to improve this point.

2.3. Mesh convergence study

A mesh convergence study has been performed to select the best parameters used in the automatic mesh generation process, and to validate the results given by the flow solver. The study has been made on the baseline BWB shape, SU2 solving the RANS equations. The aerodynamic conditions are presented Table 3. They are representative of the cruise segment, as computed by the OAD process. All the meshes are generated with a first cell height so that y+≈1 on the BWB surface. Figure 6 shows an overview of a mesh having 37 millions of elements. This is the mesh that has been retained for the RANS computations presented in Section 4.

Table 3. Aerodynamic cruise conditions

Mach	0.78
Altitude	12636 m
Reynolds per meter	4.7779*10⁶

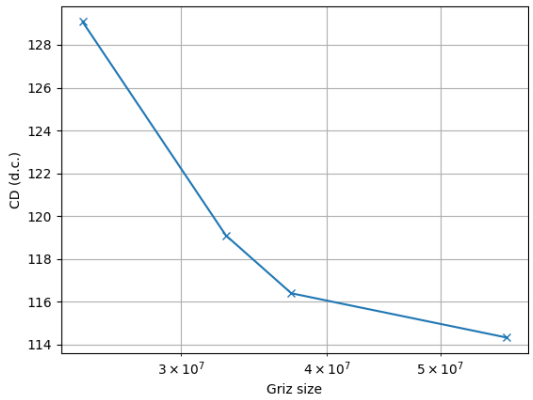

Figure 5. Mesh convergence of the drag coefficient on the baseline configuration at cruise conditions

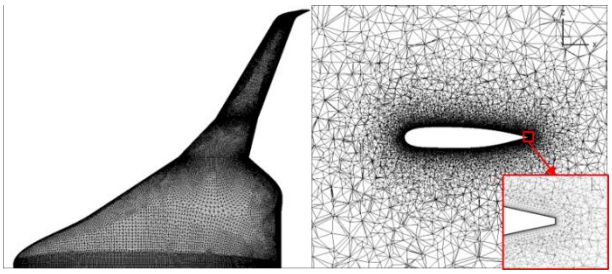

Figure 6. Unstructured mesh having 37M of elements, used for RANS evaluations

3. OPTIMIZATION PROBLEM

3.1. Geometric parametrization

In order to obtain an efficient form, the BWB geometry has been parameterized, to allow its modification and its complete definition by a finite set of parameters. A large part of these parameters are fixed by the planform. The planform was optimized by the OAD process; it is then considered as optimal, explaining why it is unchanged in this work. As seen in Figure 4, the BWB is defined using six sections. The choice was made to parameterize the airfoils using the Class Shape Transform (CST) parameterization [16]. This method uses Bernstein polynomials weighted by a shape function to define completely the upper and lower side of the airfoil. Because of the use of finite differentiation and to limit the computational cost, each airfoil is parameterized using only eight CST coefficients (four on each side). The other parameters not fixed by the planform are the twist angles on each section. Finally, the winglet geometry is kept fixed, its shape being defined by lofting the last airfoil “p3” (see Figure 4). The angle of attack is also left free to respect the lift coefficient constraint.

In total, the optimization problem can use 55 design variables to modify the aircraft shape:

- 6*8 = 48 for the airfoils shapes
- 6 twist angles
- 1 angle of attack

The main geometric constraint is represented in Figure 4 by the internal pressurized volume in red. The dimensions of this volume has been fixed by the OAD process. Some margins have been added to account for the aircraft structure, allowing using this volume directly as a geometric constraint. ESP allows computing the intersectional volume between the exterior shape and the internal one. This value in then extracted to constrain the optimization process.
On the outer wing section, only a minimum relative thickness constraint is used, on the three sections considered.

3.2. Optimizations

The optimization aiming at improving the aerodynamic efficiency, the objective is naturally to minimize the aircraft drag coefficient (CD), while maintaining a sufficient lift level. In our case, as the OAD process gives the aircraft mass balance and reference surface, it fixes the cruise lift coefficient (CL) at a value of 0.273. The same process also fixes the cruise aerodynamic conditions (see Table 3).
In addition to the lift constraint, as a BWB aircraft does not have any tail stabilizer, a trim constraint is thus added. To do so, at the lift value considered, the longitudinal moment coefficient computed at the centre of gravity (Cm_{cog}) should be zero. This ensures that the centre of pressure coincides with the centre of gravity, implying that the aircraft is trimmed during cruise without the need to deflect any control surface, which would cause a drag penalty. The position of the centre of gravity is considered constant, as no modification of the planform is made during the optimization. For the optimization process, the position of the centre of gravity is a mean positon during cruise, as computed by the OAD process. This process also provides the centre of gravity for various aircraft load, notably zero fuel weight (ZFW) and with max fuel weight and max payload weight (MFW). The trim conditions were re-computed a posteriori for these two other centre of gravity positions.

Static margin has been computed and found positive around 2% of the mean aerodynamic chord for the baseline configuration. Since no modification of the planform is done during the optimization process, no constraint is applied on this criterion. A posteriori evaluation is made, to check the stability of the optimized design.

As highlighted in previous works [1][2], the challenge posed by the BWB configuration manly lies in the central body. The need for a moderate angle of attack is implemented in the optimization problem by bounding the angle of attack variable.

Only the cruise conditions were considered (single point optimization). A low-speed evaluation of the current design should be added to the presented work, notably to check the take-off rotation criteria, as mentioned in [3].

As the number of design variables is quite important and since finite differences are used to evaluation the sensitivities, three optimizations have been run successively, optimizing only subsets of the design variables at each step. The choice of the parameters and constraints on each optimization has been made after analysing carefully each resulting design, and identifying which areas could be improved.

The three optimization problems are described below:

Optimization 1 (outer wing and twist law):

20 design variables:
- 16 CST parameters to describe airfoil shapes p2 and p21
- 3 twist angles (sections p2, p21 and p3) $\in [-6°, 6°]^3$
- 1 angle of attack < 3.5°

Objective : Minimize inviscid drag coefficient CD
Constraints:
- $CL \geq CL_{cruise}$
- $(t/c)_{p2} \geq 0.12$
- $(t/c)_{p21} \geq 0.10$

Optimization 2 (central body and twist law):

28 design variables:
- 24 CST parameters to describe airfoil shapes p0, p01 and p1
- 3 twist angles (sections p2, p21 and p3) $\in [-6°, 6°]^3$
- 1 angle of attack < 3.5°

Objective : Minimize inviscid drag coefficient CD
Constraints:
- $CL \geq CL_{cruise}$
- $Cm_{cog} \geq 0.0$
- $Exceeding\ Volume < 0.0$

Optimization 3 (central body):

24 design variables:
- 24 CST parameters to describe airfoil shapes p0, p01 and p1

Objective : Minimize inviscid drag coefficient CD
Constraints:
- $CL \geq CL_{cruise}$
- $Cm_{cog} \geq 0.0$
- $Exceeding\ Volume < 0.0$

4. GLIDER OPTIMIZATION

The results of the three optimizations described above are presented in Figure 8. Only the angles of attack were modified before starting the next optimization step, to start from a point where the lift constraint was satisfied.

It can be seen that the first optimization, where the trim constraint was not active, allowed to improve the L/D ratio by almost one count. Then, the next two optimizations achieve the reduction of the moment coefficient. Figure 10 presents the polar comparison of the two configurations, evaluated with RANS computations. The bottom panel of Figure 10 shows the moment coefficient computed for three different positions of the centre of gravity. Slopes of these curves remain negative, meaning a positive static margin, which ensures a stable aircraft. It can be seen that the trim condition is not totally satisfied for the mean position of the centre of gravity (solid line), the moment coefficient having a slight negative value. Further optimizations have been performed to improve this point, but they have only be realized at the price of worst L/D ratio or higher cruise angle of attack. Since the trim condition varies quite a lot with the variation of the aircraft weight, which induces a displacement of the centre of gravity by approximatively one meter, the obtained configuration was dubbed satisfying.

On the top panel of Figure 10, it can be seen that the wave drag has been reduced by two drag counts at the cruise lift coefficient. This can be also seen in Figure 7, where high-pressure zones are reduced on the outer wing of the optimized design. Figure 9 also shows a reduced pressure peak on the outer wing (y/b = 0.8), compared to the baseline geometry.

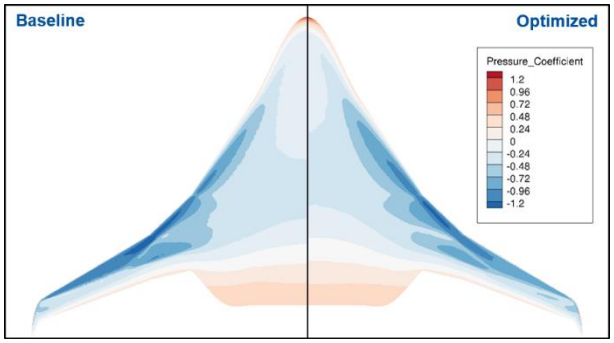

Figure 7. Pressure coefficient comparison on the baseline and optimized configurations, at cruise condition

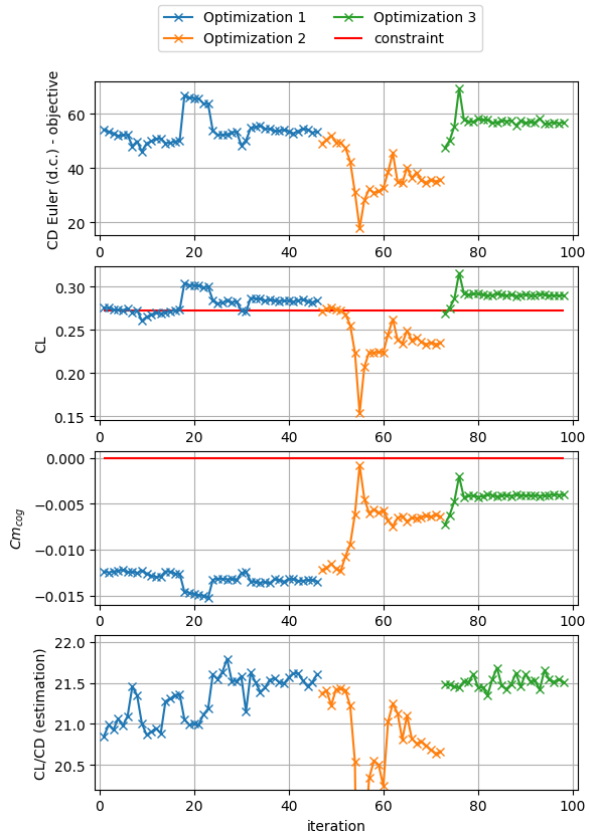

Figure 8. Evolution of the Euler drag coefficient, lift coefficient, moment coefficient and estimated L/D ratio along the optimization iterations

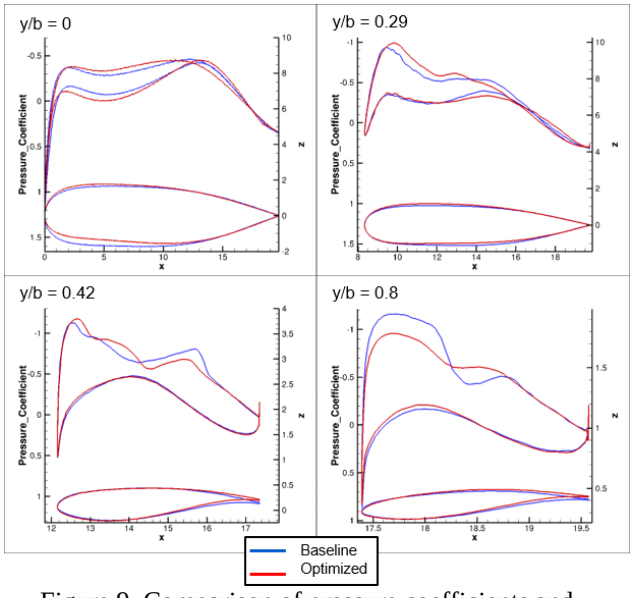

Figure 9. Comparison of pressure coefficients and airfoils on four spanwise locations of the baseline and optimized configurations.

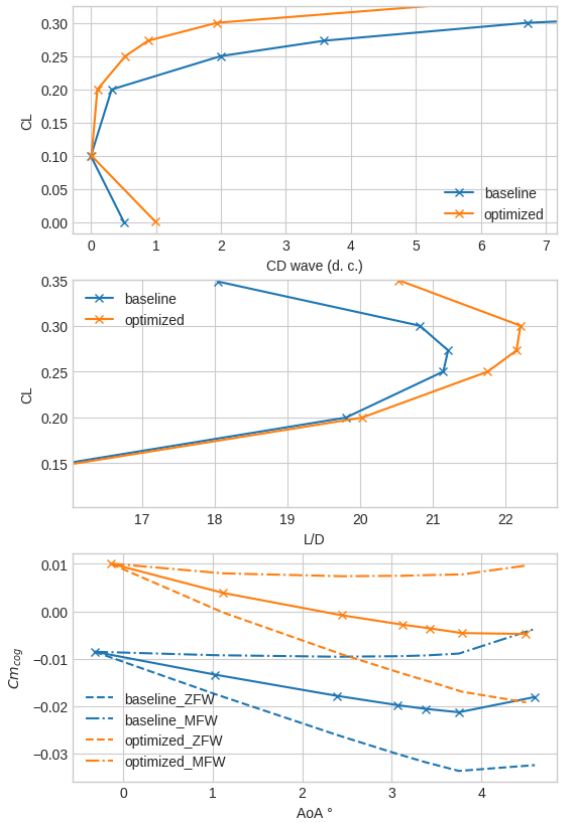

Figure 10. Comparison of the baseline and optimized geometries, using RANS computations

5. ENGINE INTEGRATION WITH BLI

The parametric modeller ESP allows exploring a great variety of design, when dealing with engine integration. The concept considered here is to integrate a high by pass ratio turbo-fan on the top of the BWB aircraft. In this position, the engines are supposed to ingest a part of the boundary layer that develops on the aircraft upper side. Boundary layer ingestion (BLI) has the capacity to provide additional fuel burn reduction compared to conventional engine installation. This was demonstrated experimentally and numerically by Carrier et al. in [17]. In a BWB context Kawai et al. [18] have shown a potential fuel burn reduction between 5 to 10 percent. Literature on BLI installation on a BWB is quite scarce, the main works having been done by NASA and Boeing in the early 2000s, including wind tunnel testing [19]. BLI allows re-energizing the boundary layers developed on the fuselage, improving the overall energy balance of the aircraft. Additional benefits lay in the reduction of the nacelle wet surface and a weight reduction due to the absence of pylons compared to a podded integration.
In the current case, the fact that a small BWB aircraft is considered, geometric constrains (mainly the internal pressurized volume) are even more pregnant than on a long range BWB.

To obtain the results presented here after, the same computational chain presented part 2.1 was used. Engines are modelled by using inlet boundary conditions in SU2, specifying density and velocity vector at the inlet and outlet of the engine. These values are obtained by using a simple thermodynamic model of a double flux turbo-fan, considering a fan pressure ratio of 1.3, representative of a modern Ultra High ByPass Ratio engine. Thrust is estimated to equilibrate the drag of a complete aircraft with an estimated L/D of 20.5. With this value, the thermodynamic model gives us the fan diameter, the pressures and mass flows, with the hypothesis of an adapted nozzle. RANS computations are again conducted, with the Spallart-Allmaras turbulence model. The boundary conditions used do not allow to account for BLI benefits (the boundary layer is lost inside the engine block). In future work, actuator disk or body force methodologies will be used to model the engine, in order to precisely quantify the effect of the BLI on the configuration. However, the current setup allows quickly spotting detached zones mainly at the inlet, the nacelle sides, and the trailing edge junction. Concerning the inlet, an S-duct shape has been employed to realize the junction between the BWB upper side and the fan face.

On the trailing edge junction, a large separation bubble can appear if the engine nozzle is significantly higher than the BWB trailing edge. This was particularly highlighted by Kim and Liou in [20] (Figure 11). This detached zone increases the overall pressure drag, and should be avoided.

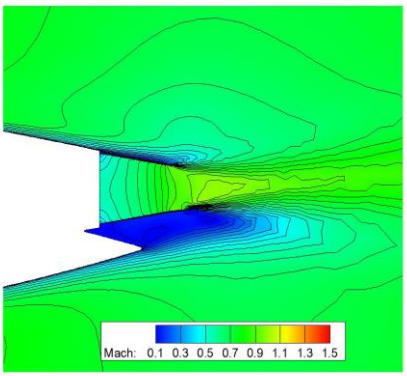

Figure 11. Separation bubble on the trailing edge region, from [20]

Figure 12 presents four different designs considered. On designs 1 and 2, the trailing edge issue has been taken into account, and the engine is positioned so that the nozzle coincides with the BWB trailing edge. Due to the simplified capabilities of ESP, Designs 1, 2 and 3 are modelled by making an union between a circular nacelle and the BWB body. An S-shape tube is then subtracted from the geometry to realize the S-duct entrance. Design 4 is a try to use a non-circular nacelle, which could prevent detaching zones appearing on the acute side

angles formed between the nacelle and the upper side of the BWB.

Figure 13 shows the Mach field in a spanwise slice containing the fan. A detached area in the S-duct appears in Design 1. Design 2 solves this issue, with a much longer S-duct. It must be stressed that the S-duct of these two designs intersects the internal pressurized volume considered in Figure 4, which violates the geometry constraint. Complying with this constraint, imply to reduce the S-duct length. Then, there is only two solutions to prevent from an abrupt slope: either move the engine upward (which would create the trailing edge issue of Figure 11) or move the engine backward. The last solution is retained in Design 3.

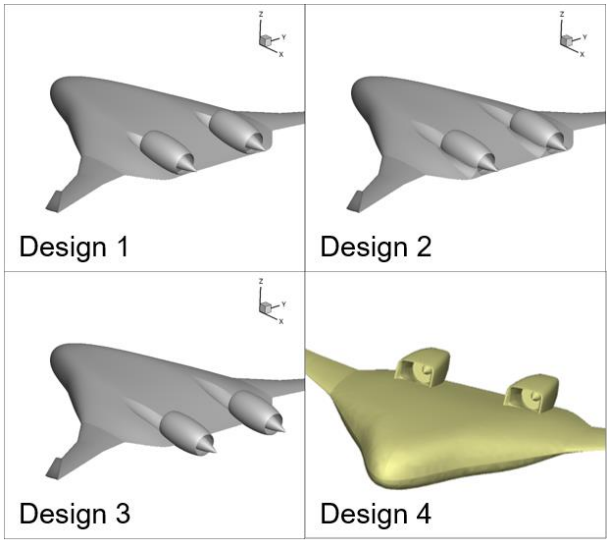

Figure 12. Overview of four different engine integration designs

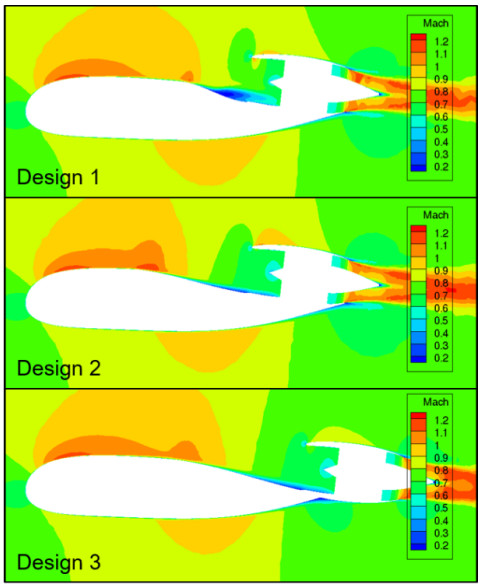

Figure 13. Comparison of Mach field between two designs, slice in the y-plane containing the fan.

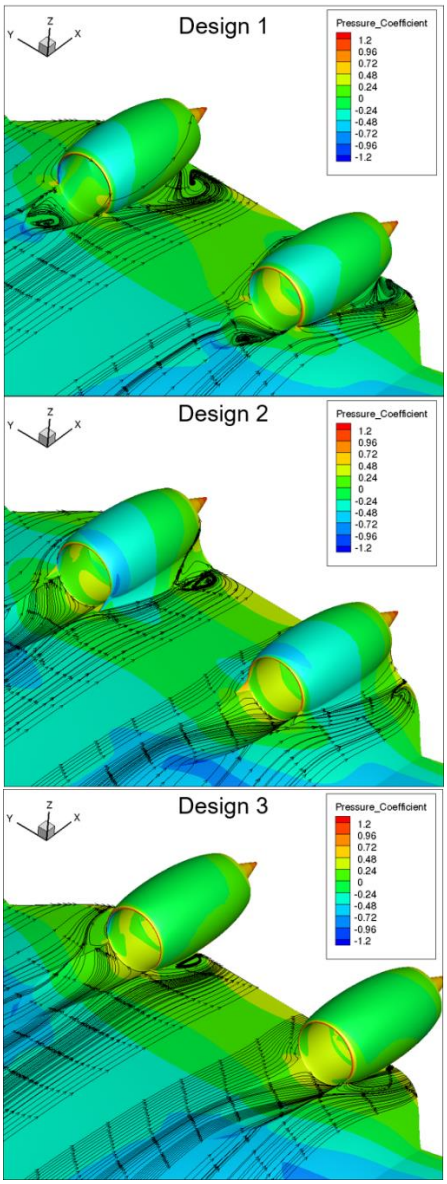

Figure 14. Pressure coefficient and friction vector on the surface of three designs considered

Figure 14 highlights that great care should be taken when designing the side junction between the nacelle and the wing. It is particularly visible that big corner separation flows are developing in these regions. Design 2 tries to solve this issue by adding fillet junction compared to Design 1. It effectively suppresses the detached zone on the external side. Because Design 3 moves the engines to the rear, the length of the acute angle is reduced, creating only a small separated bubble, even if the geometry has no fillet. Thus, Design 3 presents several advantages compared to the two others, regarding the aerodynamic performance. However, it must be stressed that the structural integration of this design appears unfavourable (see Figure 13), compared to Designs 1 and 2. A fourth different configuration (Design 4) is currently under conception and evaluation.

6. CONCLUSION

This study demonstrates the viability of the Blend Wing Body concept for a short medium range aircraft. An aerodynamic glider with a lift over drag ratio of 22 was designed, which places it at the forefront of aerodynamic efficiency on this aircraft segment. This study also demonstrated the capabilities of the new ONERA design and optimization chain, based on the geometric modeller ESP. The chain demonstrated good performance and robustness on this particular case, although no complete adjoint capability are currently available. This restricts gradient computation to finite difference and thus to Euler computation given the computing resources limitation. A complementary study with an adjoint capability could allow for RANS based optimization with a higher number of design variables at different flight points, further improving the configuration presented in this paper. The first design iterations of engine integration with BLI highlight the different challenges posed by this configuration, notably at the S-duct entrance, on the nacelle sides and at the trailing edge junction. In the near future, the design of the configuration using BLI engines is going to be finalized. Then, on this configuration, the BLI gains are going to be evaluated and quantified. Ultimately, these gains will be integrated in the OAD process, to be able to account for the BLI effects at the design stage.

7. ACKNOWLEDGEMENTS

The project leading to this application has received funding from the Clean Sky 2 Joint Undertaking under the European Union's Horizon 2020 research and innovation program under grant agreement N°CS2-AIR-GAM-2022-2023-01. The author would like to thank the project partners from DLR, Dassault Aviation and AIRBUS for their interest in this topic and their guidance.

8. REFERENCES

1. Liebeck, R. H. (2004). Design of the blended wing body subsonic transport. Journal of aircraft, 41(1), 10-25.

2. Lyu, Z., & Martins, J. R. (2014). Aerodynamic design optimization studies of a blended-wing-body aircraft. *Journal of Aircraft*, *51*(5), 1604-1617.

3. Meheut, M., Arntz, A., & Carrier, G. (2012, June). Aerodynamic shape optimizations of a blended wing body configuration for several wing planforms. In *30th AIAA Applied Aerodynamics Conference* (p. 3122).

4. Wilkerson, J. T., Jacobson, M. Z., Malwitz, A., Balasubramanian, S., Wayson, R., Fleming, G., ... & Lele, S. K. (2010). Analysis of emission data from global commercial aviation: 2004 and 2006. *Atmospheric Chemistry and Physics*, *10*(13), 6391-6408.

5. Kanazaki, M., Hanida, R., Nara, T., Shibata, M., Nomura, T., Murayama, M., & Yamamoto, K. (2013). Challenge of design exploration for small blended wing body using unstructured flow solver. *Computers & Fluids*, *85*, 71-77.

6. Gauvrit-Ledogar, J., Defoort, S., Tremolet, A., & Morel, F. (2018). Multidisciplinary overall aircraft design process dedicated to blended wing body configurations. In *2018 Aviation Technology, Integration, and Operations Conference* (p. 3025).

7. Moens, F. (2022). A L0 aerodynamic model for aircraft multidisciplinary design and optimization process. In 56th 3AF *International Conference on Applied Aerodynamics.*

8. Haimes, R., Dannenhoffer, J., Bhagat, N. D., & Allison, D. L. (2016). Multi-fidelity geometry-centric multi-disciplinary analysis for design. In *AIAA Modeling and Simulation Technologies Conference* (p. 4007).

9. Haimes, R., & Dannenhoffer, J. (2013). The engineering sketch pad: A solid-modeling, feature-based, web-enabled system for building parametric geometry. In *21st AIAA Computational Fluid Dynamics Conference* (p. 3073).

10. Karman, S. L., & Wyman, N. J. (2019). Automatic unstructured mesh generation with geometry attribution. In *AIAA Scitech 2019 Forum* (p. 1721).

11. Economon, T. D., Palacios, F., Copeland, S. R., Lukaczyk, T. W., & Alonso, J. J. (2016). SU2: An open-source suite for multiphysics simulation and design. *Aiaa Journal*, *54*(3), 828-846.

12. Cambier, L., Heib, S., and Plot, S. (2013). The Onera elsA CFD Software: Input from Research and Feedback from Industry. *Mechanics and Industry*, Vol. 14, No. 3, 2013, pp. 159–174.

13. Destarac, D. (2008). Drag extraction from numerical solutions to the equations of fluid dynamics: the far-field philosophy. *Maîtrise de la traînée et de l'impact sur l'environnement, 43ème Congrès d'Aérodynamique Appliquée de la 3AF*.

14. Vanderplaats G. N., "DOT user's manual", version 4.20, 1995

15. Wiart, L., Atinault, O., Grenon, R., Paluch, B., & Hue, D. (2015). Development of NOVA aircraft configurations for large engine integration studies. In *33rd AIAA Applied Aerodynamics Conference* (p. 2254).

16. Kulfan, B. M. (2008). Universal parametric geometry representation method. *Journal of aircraft*, *45*(1), 142-158.

17. Carrier, G., Atinault, O., Grenon, R., & Verbecke, C. (2013). Numerical and experimental aerodynamic investigations of boundary layer ingestion for improving propulsion efficiency of future air transport. In *31st AIAA Applied Aerodynamics Conference* (p. 2406).

18. Kawai, R. T., Friedman, D. M., and Serrano, L. (2006) "Blended Wing Body (BWB) Boundary Layer Ingestion (BLI) Inlet Configuration and System Studies," NASA CR-2006-214534.

19. Carter, M. B., Campbell, R. L., Pendergraft Jr, O. C., Friedman, D. M., & Serrano, L. (2006). Designing and testing a blended wing body with boundary-layer ingestion nacelles. Journal of aircraft, 43(5), 1479-1489.

20. Kim, H. J., & Liou, M. S. (2012). Optimal Inlet Shape Design of N2B Hybrid Wing Body Configuration. In 48th AIAA/ASME/SAE/ASEE Joint Propulsion Conference & Exhibit (p. 3917).